CDDpress

www.nature.com/cdd

ARTICLE

Check for updates

YTHDC1 as a tumor progression suppressor through modulating FSP1-dependent ferroptosis suppression in lung cancer

Shuai Yuan[1,7], Shu Xi[1,7], Hong Weng[1,7], Meng-Meng Guo[1], Jin-Hui Zhang[1], Zhi-Ping Yu[1], Haozhe Zhang[2], Zhaojun Yu[3], Zengzhen Xing[2], Meng-Yang Liu[1], Dao-Jing Ming[1], Rajiv Kumar Sah[2], Yi Zhou[2], Gang Li[4], Tao Zeng[3], Xin Hong[2,5], Yafei Li[6,8]✉, Xian-Tao Zeng[1,8]✉ and Hailiang Hu[2,5,8]✉

Ferroptosis is a regulated cell death process initiated by iron-dependent phospholipid peroxidation and is mainly suppressed by GPX4-dependent and FSP1-dependent surveillance mechanisms. However, how the ferroptosis surveillance system is regulated during cancer development remains largely unknown. Here, we report that the YTHDC1-mediated m^{6}A epigenetic regulation of FSP1 alleviates the FSP1-dependent ferroptosis suppression that partially contributes to the tumor suppressive role of YTHDC1 in lung cancer progression. YTHDC1 knockdown promoted the lung tumor progression and upregulated FSP1 protein level that resulted in ferroptosis resistance of lung cancer cells. Silencing FSP1 abrogated YTHDC1 knockdown-induced proliferation increase and ferroptosis resistance. Mechanistically, YTHDC1 binding to the m^{6}A sites in the *FSP1* 3′-UTR recruited the alternative polyadenylation regulator CSTF3 to generate a less stable shorter 3′-UTR contained *FSP1* mRNA, whereas YTHDC1 downregulation generated the longer 3′-UTR contained *FSP1* mRNA that is stabilized by RNA binding protein HuR and thus led to the enhanced FSP1 protein level. Therefore, our findings identify YTHDC1 as a tumor progression suppressor in lung cancer and a ferroptosis regulator through modulating the *FSP1* mRNA stability and thus suggest a ferroptosis-related therapeutic option for YTHDC1^{high} lung cancer.

Cell Death & Differentiation (2023) 30:2477–2490; https://doi.org/10.1038/s41418-023-01234-w

INTRODUCTION

Ferroptosis is a form of regulated cell death induced by iron-dependent lipid peroxidation [1] and cancer cells have evolved multiple surveillance mechanisms to escape ferroptosis and progress to advanced stages [2]. GPX4 and FSP1 are two major ferroptosis surveillance proteins that detoxify lipid hydroperoxides, either via reduction of phospholipid hydroperoxides (PLOOHs) to corresponding alcohols (PLOHs) or via reduction of ubiquinone to ubiquinol, respectively [3, 4]. FSP1, previously known as a p53-induced target protein [5], suppresses ferroptosis by catalyzing the regeneration of CoQ_{10} using NAD(P)H in a GPX4-independent manner [6, 7]. Although ferroptosis has been shown to be involved in multiple diseases, little is known about how these two ferroptosis surveillance proteins are regulated during cancer development.

The N6-methyladenosine (m^{6}A) modification of RNA is capable of regulating many RNA processes, such as splicing, polyadenylation, nuclear export, and translation, through m^{6}A "writers" (methyltransferases), "erasers" (demethylases) and "readers" [8]. Most m^{6}A "readers" contain the YTH (YT521-B homology) domain to bind m^{6}A modified sites [9, 10] and YTHDC1 is known as the YTH domain-containing nuclear reader and exerts its multifaceted effects to determine the fates of m^{6}A-marked mRNA in the nucleus [11]. As a result, YTHDC1 plays an essential role in normal physiological development processes, such as guarding the identity of mouse embryonic stem cells [12, 13] and ensuring the appropriate mouse oocyte development [14]. In addition, YTHDC1 plays different roles in cancers, such as promoting leukemogenesis as an oncogene [15] and predicting the prognosis of endometrial cancer as a biomarker [16]. Interestingly, YTHDC1 is able to form YTHDC1-m^{6}A condensates through liquid-liquid phase separation to prevent the degradation of m^{6}A-mRNAs that leads to their oncogenic activity in myeloid leukemia [17]. Although YTHDC1 has been reported to mediate the function of several oncogenes or tumor suppressors as an m^{6}A reader [18, 19], the specific role and mechanism of YTHDC1 in lung cancer development remains largely elusive.

In this study, we identify YTHDC1 as a tumor progression suppressor in lung cancer and demonstrate that the modulation of the FSP1-dependent ferroptosis activity by YTHDC1 partially contributes to its tumor progression suppressor's activity.

[1]Center for Evidence-Based and Translational Medicine, Zhongnan Hospital of Wuhan University, Wuhan, China. [2]Department of Biochemistry, School of Medicine, Southern University of Science and Technology, Shenzhen, China. [3]Department of Urology, The Second Affiliated Hospital of Nanchang University, Nanchang, China. [4]Cancer Center, Faculty of Health Sciences, MoE Frontier Science Center for Precision Oncology, University of Macau, Taipa, Macau, SAR, China. [5]Key University Laboratory of Metabolism and Health of Guangdong, Southern University of Science and Technology, Shenzhen, China. [6]Department of Epidemiology, College of Preventive Medicine, Army Medical University, Chongqing, China. [7]These authors contributed equally: Shuai Yuan, Shu Xi, Hong Weng. [8]These authors jointly supervised this work: Yafei Li, Xian-Tao Zeng, Hailiang Hu. ✉email: liyafei2008@hotmail.com; zengxiantao1128@whu.edu.cn; huhl@sustech.edu.cn

Received: 9 January 2023 Revised: 8 October 2023 Accepted: 17 October 2023
Published online: 30 October 2023

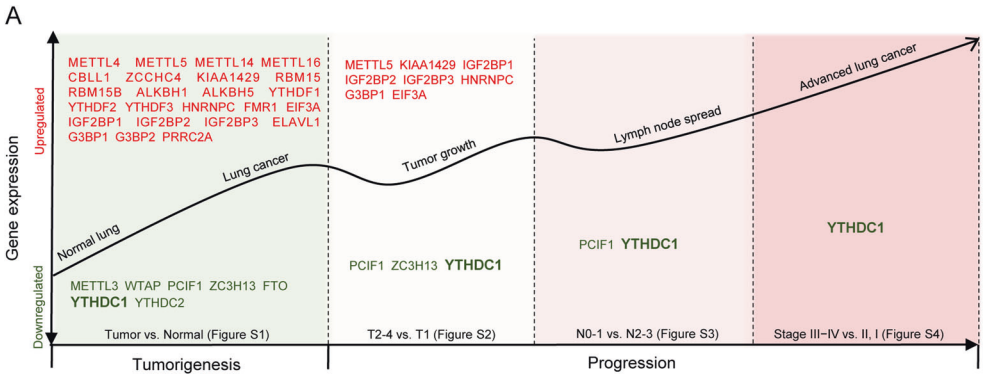

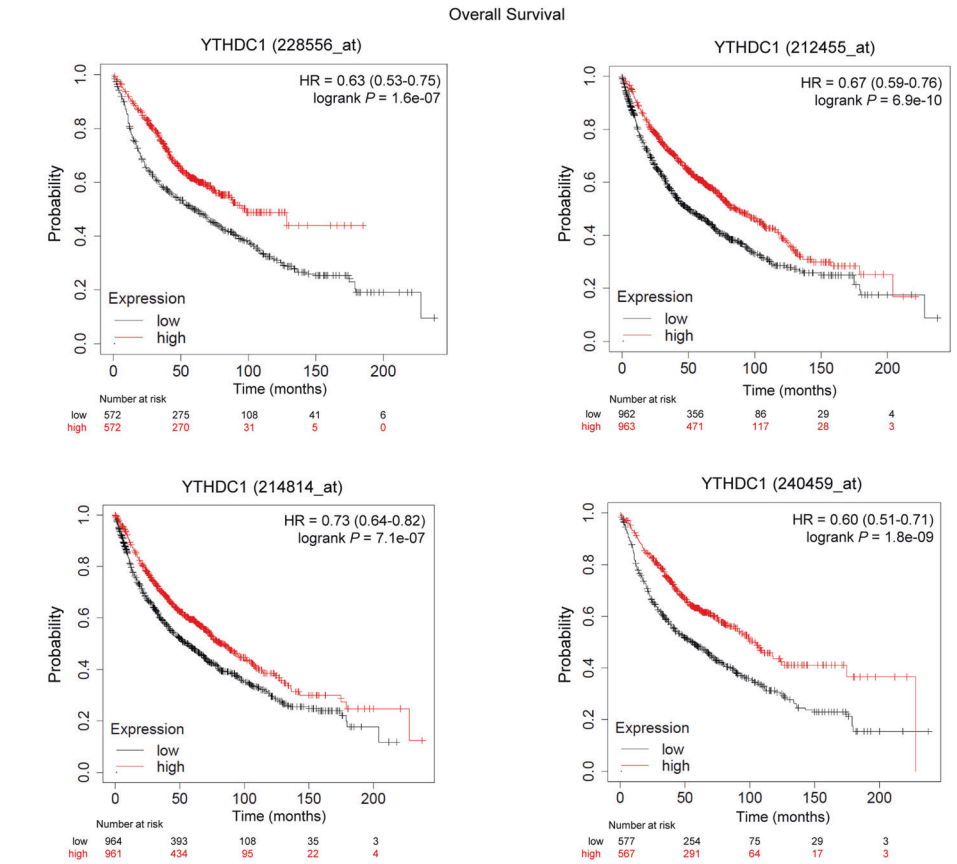

C

Factor	228556_at		212455_at		214814_at		240459_at	
	P	HR (95% CI)	*P*	HR (95% CI)	*P*	HR (95% CI)	*P*	HR (95% CI)
Stage	0.0000	2.47 (1.82 - 3.35)	0.0000	1.84 (1.51 - 2.25)	0.0000	1.85 (1.51 - 2.26)	0.0000	2.40 (1.78 - 3.24)
Gender	0.1153	1.40 (0.92 - 2.14)	0.0813	1.32 (0.97 - 1.81)	0.0171	1.48 (1.07 - 2.03)	0.1677	1.34 (0.88 - 2.03)
Smoking history	0.1477	0.68 (0.41 - 1.14)	0.1614	0.72 (0.45 - 1.14)	0.3285	0.79 (0.49 - 1.27)	0.1693	0.70 (0.42 - 1.17)
YTHDC1	0.0026	0.55 (0.38 - 0.81)	0.0010	0.59 (0.43 - 0.81)	0.0001	0.51 (0.37 - 0.71)	0.0097	0.60 (0.41 - 0.88)

RESULTS

YTHDC1 is negatively correlated with the progression of lung cancer patients

It has been known that the dysregulation of RNA m^{6}A modification by its regulators is critical for cancer initiation and progression [20]. To systematically screen the expression patterns of m^{6}A "writers", "erasers" and "readers" along the tumor progression of lung cancer, we analyzed The Cancer Genome Atlas (TCGA) and Genotype-Tissue Expression (GTEx) databases and found that among the 32 m^{6}A modification-related genes, 24 genes were

Fig. 1 YTHDC1 is negatively correlated with the progression of lung cancer. A The expression patterns of m^{6}A "writers" (METTL3, METTL4, METTL5, METTL14, METTL16, WTAP, KIAA1429, RBM15, RBM15B, ZC3H13, CBLL1, ZCCHC4, and PCIF1), "erasers" (ALKBH1, ALKBH5, and FTO) and "readers" (YTHDC1, YTHDC2, YTHDF1, YTHDF2, YTHDF3, HNRNPA2B1, HNRNPC, FMR1, EIF3A, IGF2BP1, IGF2BP2, IGF2BP3, ELAVL1, G3BP1, G3BP2, and PRRC2A) along the tumor progression of lung cancer are analyzed using the GTEx Portal (version V8) and TCGA (version 2019-7-20) databases. **B** Kaplan–Meier curves for overall survival of lung cancer patients with high and low expression levels of YTHDC1 using the Kaplan–Meier Plotter (KMplot) program (www.kmplot.com, version 2022). The median gene expression values as the cutoff. Four probes (228556_at, 212455_at, 214814_at and 240459_at) targeting YTHDC1 are used. **C** The association between YTHDC1 with overall survival in lung cancer is analyzed using multivariate Cox proportional-hazards regression analysis after adjustment for tumor stage, gender, and smoking history. Four probes (228556_at, 212455_at, 214814_at and 240459_at) targeting YTHDC1 are used.

upregulated and 7 genes were downregulated in the lung cancer tissues compared to the normal tissues, and YTHDC1 is one of the downregulated genes (Fig. 1A, Supplementary Fig. S1). Further analysis using TCGA database revealed that 8 of those 24 upregulated genes were continuously upregulated and 3 of those 7 downregulated genes, including YTHDC1, were consistently downregulated in T2-4 tumors compared to T1 tumors (Fig. 1A, Supplementary Fig. S2). Interestingly, PCIF1 and YTHDC1 were still downregulated in N2-3 tumor tissues with lymph node spread compared with N0-1 tumor tissues (Fig. 1A, Supplementary Fig. S3), and YTHDC1 is the only one gene that was gradually decreased with the progression of lung cancer from stage I to the advanced stage III-IV (Fig. 1A, Supplementary Fig. S4). Therefore, these analyses revealed that YTHDC1 was the only m^{6}A modification regulator that was persistently decreased during the initiation and progression of lung cancer (Fig. 1A), suggesting a potential tumor suppressive role for YTHDC1 in lung cancer progression.

To further assess the clinical relevance of YTHDC1 in lung cancer patients, we performed a meta-analysis to assess the association of YTHDC1 expression with outcomes of lung cancer patients using the Kaplan–Meier Plotter (KMplot) program. Using median gene expression values as the cutoff, we observed low expression of YTHDC1 was significantly associated with worse overall survival in patients with lung cancer (Fig. 1B). This association remains significant by a multivariate Cox proportional-hazards regression analysis after adjustment for tumor stage, gender, and smoking history (Fig. 1C). Taken together, these data suggest that YTHDC1 may function as a tumor progression suppressor in lung cancer.

YTHDC1 downregulation promotes lung cancer progression

To verify the findings obtained from those bioinformatics and clinical analyses, we examined YTHDC1 protein levels in 95 lung tumor tissues (Supplementary Table S1) by immunohistochemical staining and divided these tumor samples into YTHDC1^{low} (immunostaining score ≤ 75) and YTHDC1^{high} (immunostaining score > 75) groups according to its nuclear staining (Fig. 2A). Kaplan–Meier analysis indicated that low level of nuclear YTHDC1 was significantly associated with worse outcome in patients with lung cancer (Fig. 2B). Although it is known as a nuclear protein, YTHDC1 was detected in both cell nucleus and cytoplasm in the lung tumor tissues. Based on the subcellular localization of YTHDC1 protein, we divided tumor samples into two groups: predominant nuclear localization (nuclear immunostaining score > cytoplasmic immunostaining score) and predominant cytoplasmic localization (nuclear immunostaining score ≤ cytoplasmic immunostaining score) (Fig. 2C). Kaplan–Meier analysis showed that predominant cytoplasm localization group had a worse prognosis of overall survival in lung cancer patients (Fig. 2D), suggesting that less nuclear YTHDC1 level is correlated with progression of lung cancer as well.

To directly evaluate the potential tumor progression suppressor activity of YTHDC1 in lung cancer, we established YTHDC1-overexpressing stable cell line by introducing Flag-tagged YTHDC1 into H460 cells (Fig. 2E), a lung cancer cell line with relatively low YTHDC1 protein levels compared to other cell lines (Supplementary Fig. S5A). Overexpression of YTHDC1 significantly decreased the proliferation and colony formation of H460 cells (Fig. 2F, G), suggesting a tumor suppressive activity of YTHDC1 in lung cancer cells. To further confirm these results, we stably knocked down YTHDC1 in A549 and H1299 cells by two independent YTHDC1 shRNAs (Fig. 2H, Supplementary Fig. S5B). YTHDC1 knockdown significantly promoted the proliferation of A549 and H1299 cells in vitro (Fig. 2I) as well as significantly increased the growth of A549 xenograft tumors and their size in vivo (Fig. 2J–L, Supplementary Fig. S5C). Taken together, the clinical and functional data indicate that YTHDC1 has a tumor suppressive role in lung cancer progression.

YTHDC1 downregulation increases the ferroptosis resistance

To explore the potential mechanisms that YTHDC1 suppressed lung cancer progression, we conducted an RNA-seq for control and stable YTHDC1-knockdown A549 cells and found 291 differentially expressed genes (DEGs), including 151 upregulated genes and 140 downregulated genes ($q < 0.05$) (Supplementary Fig. S5D, Supplementary Table S2). KEGG (Kyoto encyclopedia of genes and genomes) pathway analysis of these DEGs revealed ferroptosis as one of the most affected cellular processes in YTHDC1-knockdown cells (Fig. 3A), and the altered genes (including *TP53*, *CP* and *SLC40A1*) in the ferroptosis category were validated by qRT-PCR in the YTHDC1 knockdown cells (Supplementary Fig. S5E). By using gene set enrichment analysis (GSEA), we found a correlation between YTHDC1 and ferroptosis activity (Fig. 3B), suggesting that YTHDC1-knockdown might lead to ferroptosis suppression in lung cancer. Although KEGG pathway analysis indicated that apoptosis was one of the affected cellular processes as well, the caspase-3 protein (a key mediator and a well-established cellular marker of apoptosis) level was not altered in YTHDC1-knockdown cells (Supplementary Fig. S5F).

To validate the association between YTHDC1 and ferroptosis activity, we knocked down YTHDC1 in A549 and H1299 cells and found that more colonies were formed in YTHDC1 knockdown cells with RSL3 treatment (Fig. 3C, D). Furthermore, both A549 and H1299 cells with YTHDC1 knockdown were more resistant to RSL3-induced ferroptosis (Fig. 3E, F; Supplementary Fig. S6A). The similar resistant results were found for both A549 and H1299 cells with YTHDC1 knockdown treated with other ferroptosis inducers, including Erastin (Fig. 3G, H), FIN56 (Supplementary Fig. S6B), and $FINO_2$ (Supplementary Fig. S6C). As ferroptosis can be indicated by enhanced *PTGS2* expression and increased ROS level [21], we found that knocking down YTHDC1 down-regulated *PTGS2* mRNA expression (Fig. 3I) and decreased the cellular ROS level upon the RSL3 treatment (Fig. 3J). Furthermore, ferroptosis is characterized morphologically by smaller mitochondria with condensed mitochondrial membrane densities, reduced or vanished mitochondria crista and ruptured outer mitochondrial membrane [22]. As shown in Fig. 3K, RSL3 treatment induced the typical morphological alterations of mitochondria, indicative of ferroptosis occurrence, whereas YTHDC1 knockdown alleviated these RSL3-induced mitochondrial changes in A549 cells.

We further directly evaluated the lipid peroxidation by using BODIPY-C11, a well-known lipid peroxidation marker. Since our

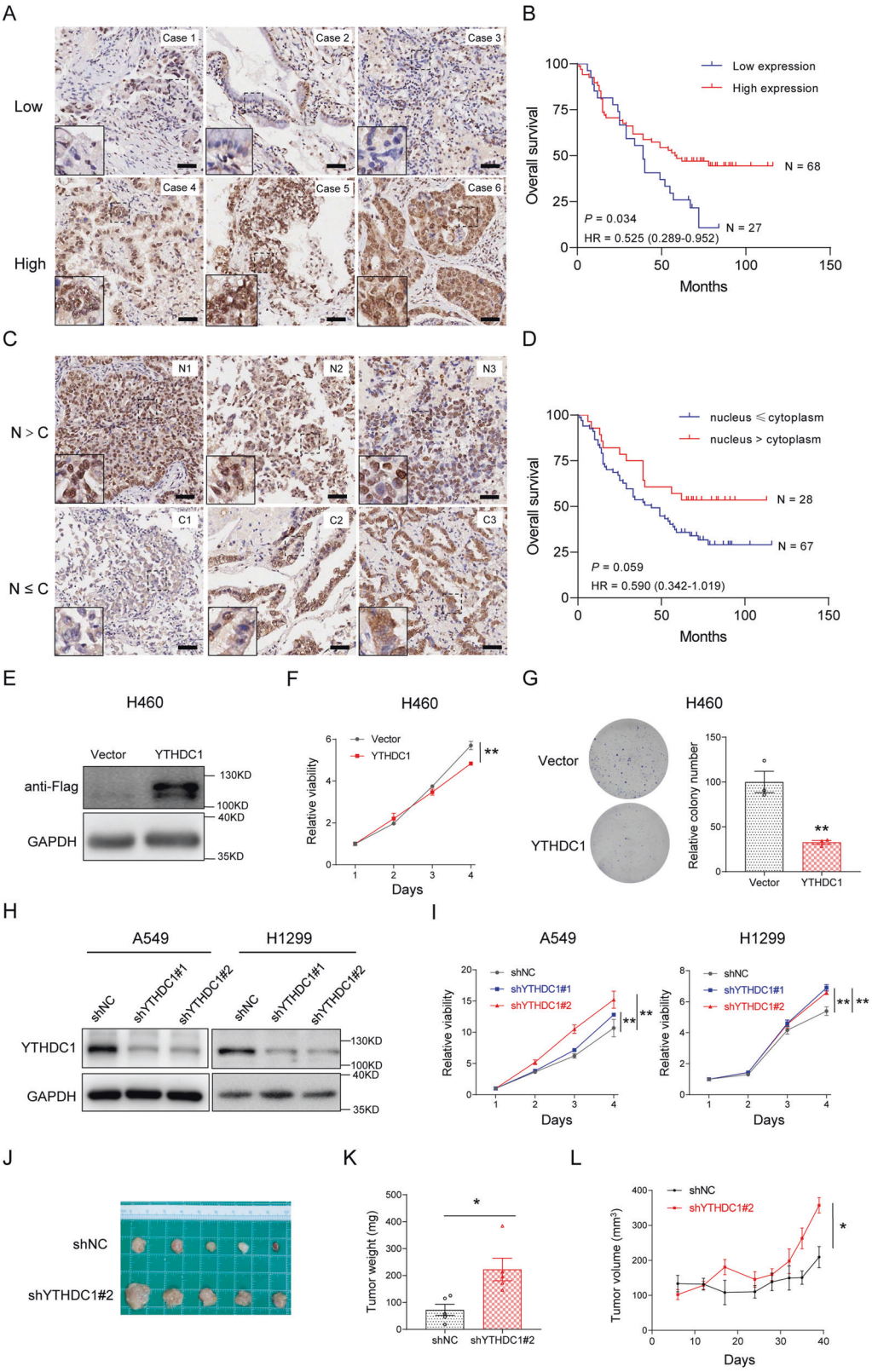

shRNA-YTHDC1 vectors contained GFP fluorescence, which interfered with the detection of lipid peroxidation with BODIPY-C11, we established the YTHDC1 knockout A549 cells using CRISPR/Cas9 (Supplementary Fig. S6D). Although we didn't select the single clone with undetectable YTHDC1 protein level, our pooled population A549 cells with YTHDC1 knockout showed a decreased lipid peroxidation level upon the RSL3 treatment and more resistant to RSL3-induced ferroptosis indicated by an increased IC50 value (Supplementary Fig. S6E, F). Therefore, YTHDC1 downregulation leads to ferroptotic resistance in lung cancer cells.

Fig. 2 YTHDC1 suppresses lung cancer progression. A Low and high protein levels of nuclear YTHDC1 in representative lung cancer tissues by immunohistochemical staining. Scale bars represent 50 μm. For each case, immunostaining score with a potential range of 0–300 is calculated as follows: Immunostaining score = [extent of positive cell staining (0–100%) × staining intensity (0–3)] × 100. High YTHDC1 protein level group contains the immunostaining score >75 patients. Low YTHDC1 protein level group contains the immunostaining score ≤75 patients. **B** Kaplan–Meier curves for overall survival of lung cancer patients ($n = 95$) with high and low protein levels of YTHDC1. **C** Representative immunohistochemical staining of lung cancer tissues with dominant nuclear (upper) or dominant cytoplasmic (lower) YTHDC1 level. Scale bars represent 50 μm. **D** Kaplan–Meier curves for overall survival of lung cancer patients ($n = 95$) with dominant nuclear and dominant cytoplasmic YTHDC1 level. **E** The protein levels of YTHDC1 are detected by WB using anti-Flag antibody in H460 cells after overexpression of Flag-tagged YTHDC1. **F** Cell proliferation is detected by CCK-8 assays after overexpression of YTHDC1 in H460 cells. The difference between cell proliferation curves is evaluated using repeated measures analysis of variance. **G** Colony formation assays are conducted after overexpression of YTHDC1 in H460 cells. **H** The knockdown effects of YTHDC1 by shRNA are detected using WB in A549 and H1299 cells. **I** Cell proliferation is detected by CCK-8 assays after stable knockdown of YTHDC1 in A549 and H1299 cells. The difference between cell proliferation curves is evaluated using repeated measures analysis of variance. **J** Subcutaneous xenograft tumors are dissected and photographed. **K** The tumor weight of A549 cells with stable knockdown of YTHDC1 or control. Results of tumor weight are evaluated using the two-tailed Student's *t*-test. **L** The tumor growth curve of A549 cells with stable knockdown of YTHDC1 or control. The difference between tumor growths curves is evaluated using repeated measures analysis of variance. $^{*}P < 0.05$; $^{**}P < 0.01$.

YTHDC1 regulates FSP1 at the post-transcriptional level in an m^{6}A-dependent manner

GPX4 and FSP1 are two independent regulators to suppress ferroptosis [23]. Interestingly, both A549 and H1299 cells with YTHDC1 knockdown showed more resistant to RSL3-induced ferroptosis (Fig. 3E, F), but more sensitive to FSP1 inhibitor iFSP1 (Fig. 4A), suggesting that YTHDC1 knockdown may differentially regulate GPX4 and FSP1 levels in lung cancer. Indeed, YTHDC1 knockdown did not simultaneously upregulate the *GPX4* and *FSP1* mRNA expression in A549 and H1299 cells (Fig. 4B), instead markedly upregulated the FSP1 protein levels (Fig. 4C). A negative correlation between the transcription levels of *YTHDC1* and FSP1 protein levels was also identified when examining cancer cell lines from the Cancer Cell Line Encyclopedia (CCLE) (Supplementary Fig. S7A). In line with these findings, we also found that overexpression of Flag-tagged YTHDC1 decreased the FSP1 protein level in H460 cells (Supplementary Fig. S7B). Taken together, these data suggest that YTHDC1 negatively regulates FSP1 protein levels.

We next explored the underlying mechanism how YTHDC1 regulates FSP1. The mRNA levels of *FSP1* were marginally increased in YTHDC1 knockdown cells (Fig. 4B), suggesting that YTHDC1 regulated the protein level of FSP1 was not at the transcriptional level. Given that YTHDC1 is an m^{6}A reader, we analyzed m^{6}A sites in *FSP1* mRNA by SRAMP prediction program and found most of the m^{6}A sites were located in the 3′-untranslated region (UTR) of *FSP1* mRNA (Fig. 4D). Actually, methylated RNA immunoprecipitation (MeRIP)-qPCR and RNA immunoprecipitation (RIP)-qPCR assays demonstrated that *FSP1* mRNA was modified by m^{6}A in both A549 and H1299 cells and *FSP1* mRNA was recognized and bound by YTHDC1 (Fig. 4E). By using siRNAs to knock down METTL3 (an m^{6}A writer) to decrease the total m^{6}A methylation level, we found that the mRNA level of *FSP1* was not changed, but the FSP1 protein level was decreased in A549 cells (Fig. 4F, G). Additionally, METTL3 knockdown partially abrogated the YTHDC1 knockdown caused upregulation of FSP1 protein (Fig. 4H). All these data suggest that YTHDC1 suppresses FSP1 at the post-transcriptional level in an m^{6}A-dependent manner.

YTHDC1 has previously been implicated in regulating gene expression at the post-transcriptional level through mediating the nuclear export or the decay of m^{6}A methylated mRNAs [24–26]. First, we found that knockdown of YTHDC1 slightly increased the nuclear fraction of *FSP1* mRNA in A549 cells (Fig. 4I), and did not disturb the nuclear fraction and cytoplasmic fraction of *FSP1* mRNA in H1299 cells (Fig. 4J), ruling out the possibility that YTHDC1 regulates FSP1 through the mRNA nuclear export. We then treated cells with Actinomycin D, an inhibitor of RNA polymerase II, to block new RNA synthesis and found that YTHDC1 knockdown enhanced the stability of *FSP1* mRNA in both A549 and H1299 cells (Fig. 4K, L), suggesting that YTHDC1 regulates the stability of *FSP1* mRNA through m^{6}A-mediated RNA decay processing.

YTHDC1 knockdown produces a longer 3′-UTR-containing *FSP1* mRNA through alternative polyadenylation

Two poly(A) sites are identified in the 3′-UTR of *FSP1* mRNA in addition to the m^{6}A sites (Fig. 4D), raising a possibility that YTHDC1 may regulate the RNA decay of *FSP1* mRNA through alternative polyadenylation (APA). To determine which poly(A) site of *FSP1* mRNA YTHDC1 uses, we designed two paired qRT-PCR primers that specifically recognized the longer 3′-UTR of *FSP1* mRNA to monitor the distal poly(A) site usage of *FSP1* mRNA (Fig. 4D). Knockdown of YTHDC1 significantly increased the levels of the longer 3′-UTR-containing *FSP1* mRNA in A549 and H1299 cells (Fig. 5A), suggesting that YTHDC1 knockdown promoted the distal poly(A) site usage to produce a longer 3′-UTR-containing *FSP1* mRNA isoform. To further investigate how YTHDC1 regulates the 3′-UTR processing, we use the STRING database (version: 11.5) to search the top 10 proteins that are predicted to physically interact with YTHDC1 and found that seven out of ten YTHDC1 binding proteins are the components of the cleavage and polyadenylation (CPA) complex [27], which has been shown to play a critical role in APA formation and regulation (Supplementary Fig. S8A). Most of the seven YTHDC1 binding CPA factors, including CSTF3, CSTF1, CPSF1, CPSF2, and FIP1L1, are reported to use the proximal poly(A) sites that result in shorter 3′-UTR-containing mRNA [28]. We showed that YTHDC1 was able to co-immunoprecipitate with CSTF3, the core CPA complex factor, in both A549 and H1299 cells (Fig. 5B). Immunofluorescent staining further confirmed that Flag-tagged YTHDC1 co-stained with CSTF3 in A549 cells (Fig. 5C). These data suggest that YTHDC1 interacts with CPA complex to promote the proximal poly(A) site usage.

HuR stabilizes the longer 3′-UTR-containing *FSP1* mRNA to enhance FSP1 protein level

Longer 3′-UTR usually leads to the decreased stability of mRNA due to harboring miRNA regulatory sites [29]. However, some longer 3′-UTRs that harbor RNA regulatory elements (such as AU-rich elements) are able to increase the mRNA stability due to the binding of RNA binding proteins (RBPs) to these regulatory elements. By using ENCORI database, we identified 87 RBPs that bind to *FSP1* mRNA (Supplementary Table S3). Gene Ontology (GO) analysis showed that the 87 RBPs were significantly enriched in mRNA 3′-UTR binding and regulating 3′-UTR-mediated mRNA stability. Among the GO terms, four proteins (HuR, HNRNPC, TARDBP and RBM10) were enriched in 3′-UTR-mediated mRNA stabilization (Supplementary Fig. S8B), which may increase the stability of *FSP1* mRNA. We then validated the binding effect of *FSP1* mRNA 3′-UTR (*FSP1* mRNA region: 1430-3137) to the HuR,

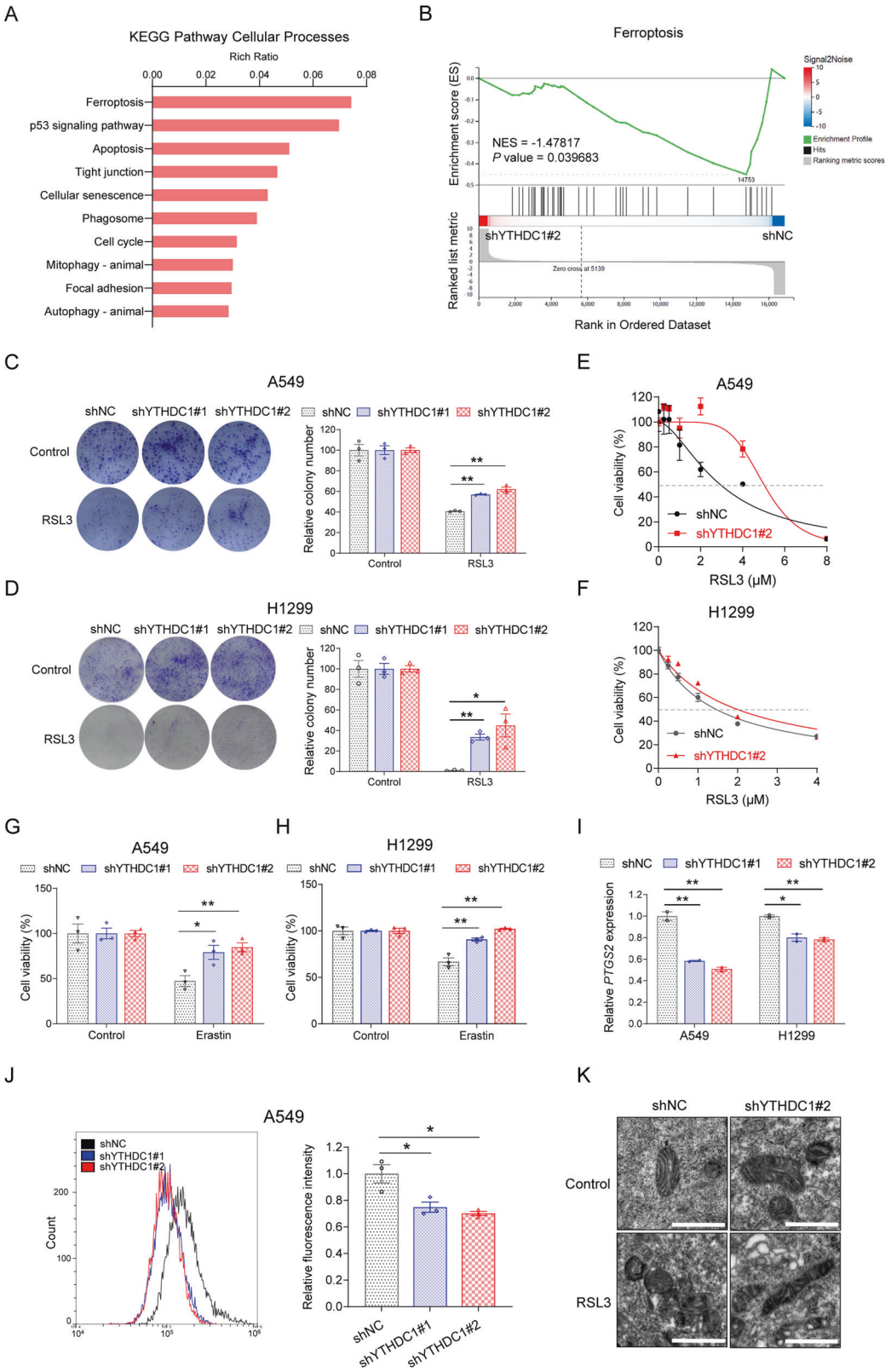

HNRNPC, TARDBP, and RBM10 proteins using catRAPID omics v2.1, and found that HuR protein showed the highest ranking of 3′-UTR binding effect (Fig. 5D). Previous studies have demonstrated that HuR was capable of stabilizing the target 3′-UTR-containing mRNA through AREs (AU-rich elements) [30]. The RIP assay confirmed that HuR was able to bind to *FSP1* mRNA in A549 cells (Fig. 5E), while knocking down HuR with siRNAs decreased stability of *FSP1* mRNA that also resulted in the decreased FSP1 protein level (Fig. 5F, G). Functionally, A549 cells with HuR knockdown were more sensitive to RSL3-induced ferroptosis (Fig. 5H), suggesting

Fig. 3 YTHDC1 promotes ferroptosis activity. A Genome-wide gene expressions are detected by RNA-seq in A549 cells with stable knockdown of YTHDC1 and Kyoto encyclopedia of genes and genomes (KEGG) pathway analysis is conducted using differentially expressed genes induced by stable knockdown of YTHDC1. **B** Gene set enrichment analysis (GSEA) shows that ferroptosis system is altered in YTHDC1 knockdown cells compared with control cells in A549 cells. **C**, **D** Colony formation assays are conducted to clarify the effect of YTHDC1 on the RSL3-induced ferroptosis in A549 and H1299 cells. Results are evaluated using the two-tailed Student's *t*-test. **E**, **F** RSL3 treatment is conducted to clarify the effect of YTHDC1 on the ferroptosis in A549 and H1299 cells. Cell proliferation is detected by CCK-8 assays and IC50 curves are generated using Graphpad Prism 8.0. **G**, **H** CCK-8 assays are conducted to clarify the effect of YTHDC1 on the Erastin-induced ferroptosis in A549 and H1299 cells. Results are evaluated using the two-tailed Student's *t*-test. **I** The expression levels of *PTGS2* are detected in A549 and H1299 cells treated with RSL3 for 48 h. Results are evaluated using the two-tailed Student's *t*-test. **J** ROS are detected by flow cytometry. A549 cells are treated with RSL3 (800 nM) for 24 h, followed by incubation with DHE for 60 min at 37 °C. Results are evaluated using the two-tailed Student's *t*-test. **K** Morphological changes of ferroptosis are detected using transmission electron microscopy. Scale bars represent 1 μm. $^{*}P < 0.05$; $^{**}P < 0.01$.

that HuR mediates the stabilization of *FSP1* mRNA and ferroptosis resistance caused by YTHDC1 knockdown.

We further mapped the binding regions of HuR to the *FSP1* mRNA. The in vitro RNA pull-down assays showed that HuR mainly interacted with the 3′-UTR of *FSP1* mRNA (Fig. 5I), which is further confirmed by the decreased binding of mutant 3′-UTR of *FSP1* mRNA to HuR proteins, wherein the three potential HuR binding sites ATTTA were mutated into AGGGA in the 3′-UTR of *FSP1* mRNA (Fig. 5J). Two luciferase reporter plasmids containing 3′-UTR of *FSP1* mRNA (wild type: ATTTA; mutant type: AGGGA) were constructed and transfected into A549 cells. As expected, the luciferase activity was significantly reduced with the knockdown of HuR for wild type luciferase reporter but not for the mutant luciferase reporter (Fig. 5K). The RIP assay further showed that knockdown of YTHDC1 increased the binding of HuR to *FSP1* mRNA (Fig. 5L). Taken together, these results demonstrate that YTHDC1 knockdown promotes the stability of *FSP1* mRNA with a longer 3′-UTR through APA, and HuR subsequently binds to the longer 3′-UTR of *FSP1* mRNA to stabilize *FSP1* mRNA and enhance its protein level.

YTHDC1 provides a ferroptotic vulnerability for lung cancer treatment

To test whether the upregulation of FSP1 mediates the tumor suppressor activity of YTHDC1 in lung cancer cells, we first examined the cell viability of YTHDC1-overexpressing H460 cells treated with ferroptosis inhibitors (Fer-1). Interestingly, the inhibiting effect of YTHDC1 on cell growth was partially restored by treating cells with Fer-1 (Supplementary Fig. S9A), whereas Fer-1 treatment did not significantly increase cell viability for vector control H460 cells and A549 cells (Supplementary Fig. S9A, B), suggesting that YTHDC1 overexpression suppresses cancer cell growth partially through ferroptosis. In parallel with this, we used siRNA to knock down FSP1 (Supplementary Fig. S9C) and found that downregulating FSP1 did decrease the proliferation of YTHDC1-knockdown A549 cells (Fig. 6A). To directly determine whether YTHDC1 modulates ferroptosis activity through FSP1. We knocked down FSP1 in A549 cells and found that FSP1 knockdown abrogated the RSL3-induced ferroptosis resistance in YTHDC1-knockdown cells (Fig. 6B), indicating that the YTHDC1-knockdown caused RSL3 resistance was mediated at least partially by the enhanced FSP1-dependent ferroptosis suppression.

The effects of YTHDC1 on ferroptosis may suggest a ferroptotic vulnerability for YTHDC1^{high} lung cancer. To test that, we first examined the YTHDC1 and FSP1 levels in four lung cancer cell lines (H1299, H1975, H460, and A549). We found that H460 cell showed the highest FSP1 level and lowest YTHDC1 level, while H1299 cell showed the lowest FSP1 level and highest YTHDC1 level (Supplementary Fig. S9D). The IC50 assay showed that H1299 cells with YTHDC1^{high} genotype were more sensitive to RSL3-induced ferroptosis than H460 cells with YTHDC1^{low} genotype (Fig. 6C), suggesting that YTHDC1^{high} lung cancer might be more susceptible for ferroptosis inducers. In line with these findings, overexpression of YTHDC1 in H460 cells increased their susceptibility to ferroptosis (Fig. 6D). To further test the effects of YTHDC1 on ferroptosis in tumor tissues, we examined the levels of 4-HNE (byproducts of lipid peroxidation) in the same 95 lung tumor tissues as above using immunohistochemical staining. We found that levels of 4-HNE in YTHDC1^{high} lung tumor tissues were higher than that in YTHDC1^{low} lung tumor tissues (Fig. 6E, F). Taken together, these data suggested that YTHDC1 increased the ferroptotic vulnerability in lung cancer.

DISCUSSION

In summary, we demonstrate in this study that YTHDC1 functions as a tumor progression suppressor in lung cancer through regulating FSP1-mediated ferroptosis suppression. Mechanistically, YTHDC1 binds to the 3′-UTR of *FSP1* mRNA that recruits APA processing factor CSTF3 to generate unstable *FSP1* mRNA isoform with shorter 3′-UTR; downregulation of YTHDC1 decreases the recruitment of CSTF3 to generate the *FSP1* mRNA isoform with longer 3′-UTR, which is subsequently stabilized by HuR to increase its protein level (Fig. 7). This mechanism may explain why YTHDC1^{low} lung cancer patients have a poor prognosis whereas YTHDC1^{high} lung cancer may have a therapeutic vulnerability for ferroptosis treatment.

YTHDC1 is identified as the mainly nuclear m^{6}A reader to control the fate of m^{6}A modified transcripts in different stages of the mRNA life cycle in the nucleus, such as mRNA splicing, transcription and nuclear export [11]. Particularly, it has been recently proposed that the formation of YTHDC1 nuclear condensates by liquid-liquid phase separation is a general mechanism to underlie its diverse functions in the nucleus [17, 31]. The tumor suppressor gene *PTEN* and oncogene *MYC* have been reported to be regulated by YTHDC1 [17, 32], indicating a differential role of YTHDC1 in cancer development. Our study here demonstrated that YTHDC1 is able to suppress lung cancer progression, at least partially, through regulating FSP1-mediated ferroptosis suppression, suggesting a new tumor suppressive role of YTHDC1 in lung cancer progression. Whether YTHDC1 functions as an authentic tumor suppressor in lung tumorigenesis, however, needs to be further investigated.

Ferroptosis is a non-apoptotic form of regulated cell death that can be triggered by phospholipid peroxidation of polyunsaturated fatty acids (PUFAs) and involved in multiple diseases such as neurodegeneration and cancer [33, 34]. Cancer cells are usually more metabolically active and tend to produce more ROS and PUFAs that make them more prone to ferroptosis [23]. However, cancer cells have evolved a variety of mechanisms to suppress ferroptosis at the genetic and epigenetic levels. GPX4 and FSP1 are the two important evolved surveillance mechanisms to protect cancer cells from ferroptosis [23]. We found that knockdown of YTHDC1 in lung cancer cells did not alter the GPX4 level, but remarkably promoted the protein level of FSP1 in an m^{6}A dependent manner, which may provide new therapeutic targets for cancers [35, 36]. A recent study reported that FSP1 was a transcriptional target of NRF2 and mediated ferroptosis-resistance

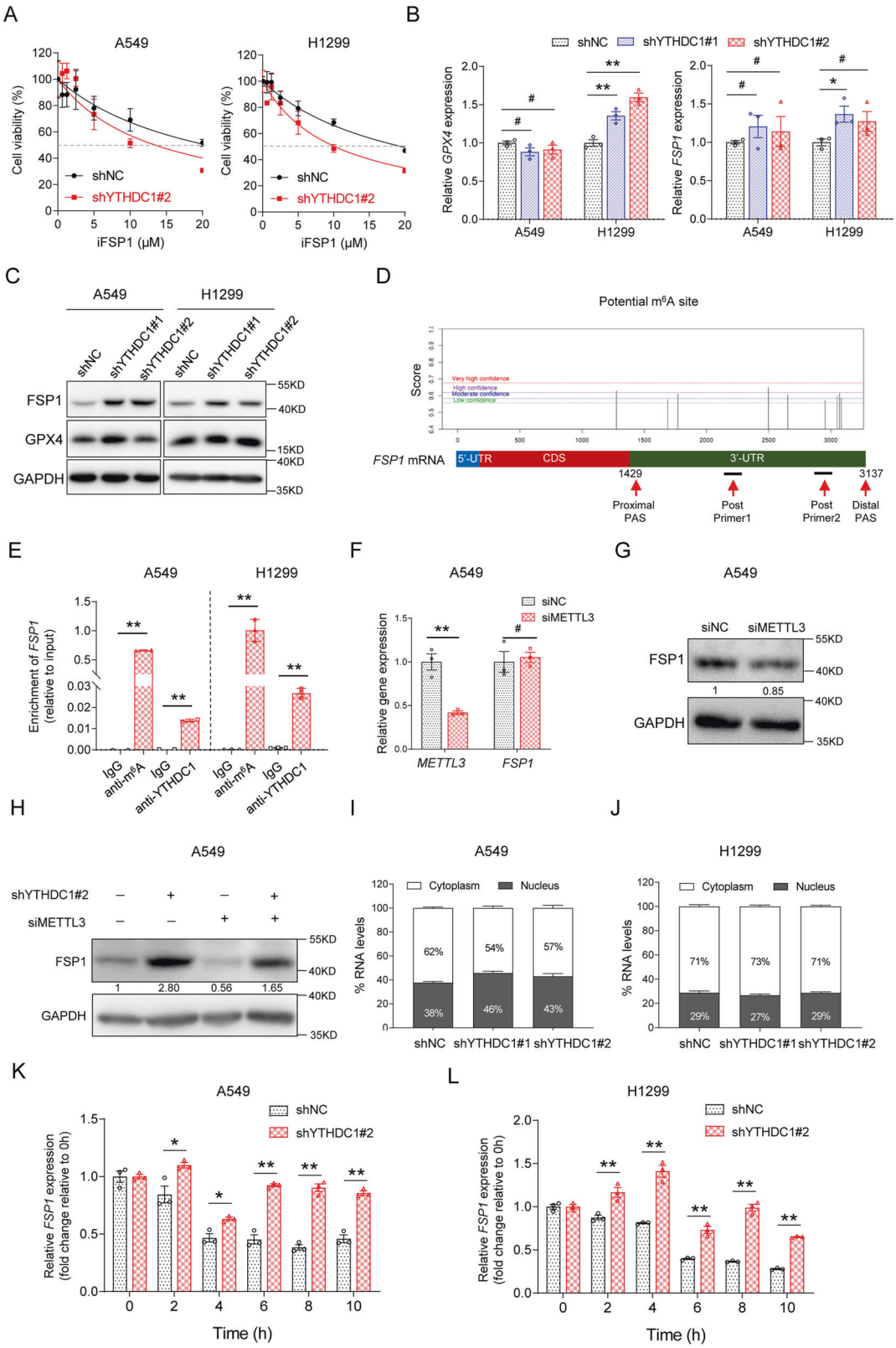

in KEAP1 deficient lung cancer cells [37]. A549 and H460 cells, two cell lines used in our study, have been reported to have mutant KEAP1 and thus exhibited high NRF2 activity and FSP1 expression. Our results showed that A549 and H460 cells harbored higher FSP1 protein levels and were more resistant to RSL3 than H1299 cells which contains wild type KEAP1. Interestingly, in addition to the regulation of *FSP1* mRNA at the transcriptional level by NRF2, our study further demonstrated that *FSP1* mRNA was regulated at the post-transcriptional level by YTHDC1 as well, which suggests another layer of FSP1 regulation.

Fig. 4 YTHDC1 regulates FSP1 at the post-transcriptional level in an m^{6}A-dependent manner. A FSP1 inhibitor iFSP1 treatment is conducted to clarify the effect of YTHDC1 on the ferroptosis in A549 and H1299 cells. Cell proliferation is detected by CCK-8 assays and IC50 curves are generated using Graphpad Prism 8.0. **B** The expression levels of *GPX4* and *FSP1* mRNA are detected by qRT-PCR in A549 and H1299 cells after knockdown of YTHDC1. Results are evaluated using the two-tailed Student's *t*-test. **C** The GPX4 and FSP1 protein levels are detected by WB in A549 and H1299 cells after knockdown of YTHDC1. **D** By using SRAMP prediction server (http://www.cuilab.cn/sramp), a mammalian m^{6}A sites predictor, we identified most of the m^{6}A sites are located in the 3′-UTR of *FSP1* mRNA. A proximal polyadenylation site (PAS) and a distal PAS are found in the NCBI Gene (https://www.ncbi.nlm.nih.gov/gene). **E** The m^{6}A RNA modification of *FSP1* mRNA and the binding effects of YTHDC1 to *FSP1* mRNA are detected by MeRIP and RIP assays in A549 and H1299 cells. **F** The expression levels of *FSP1* mRNA are detected by qRT-PCR in A549 after knockdown of METTL3. **G** The FSP1 protein levels are detected by WB in A549 cells after knockdown of METTL3. The numbers represent the quantification results of the WB. **H** Rescue effect of siMETTL3 on the upregulation of FSP1 protein induced by YTHDC1 knockdown in A549 cells. The numbers represent the quantification results of the WB. **I**, **J** The nuclear and cytoplasmic fractions of *FSP1* mRNA are detected by qRT-PCR after knockdown of YTHDC1 in A549 and H1299 cells. **K**, **L** Stability of *FSP1* mRNA over 10 h is measured by qRT-PCR relative to time 0 h after blocking new RNA synthesis with Actinomycin D (5 μg/mL) in A549 and H1299 cells with stable knockdown of YTHDC1. Results are evaluated using the two-tailed Student's *t*-test. $^{\#}P > 0.05$; $^{*}P < 0.05$; $^{**}P < 0.01$.

APA is a widely-used gene regulation mechanism for many cellular functions [38] and dysregulation of APA contributes to the development of various diseases, including cancer [39]. A most recent study showed that APA events with more longer isoforms are found in Ythdc1-deficient oocytes [14]. In consistent with these results, we identified that YTHDC1 is able to regulate the stability of *FSP1* mRNA through APA and knockdown of YTHDC1 increased the abundance of *FSP1* mRNA isoforms with longer 3′-UTR. Usually longer 3′-UTR containing mRNA tends to have a decreased stability due to the miRNA regulatory sites in the mRNA 3′-UTR region [29, 40]. However, several mRNAs with longer 3′-UTRs have increased mRNA stability due to the AREs in the 3′-UTR, which can recruit HuR protein and stabilize the target longer 3′-UTR isoforms through ARE-mediated stabilization [29, 41]. Our study showed that the longer 3′-UTR of *FSP1* mRNA harbored ARE sites and can be stabilized by the HuR binding, therefore increasing the FSP1 protein levels in YTHDC1 knockdown cells. Loss of YTHDC1 has been shown to alter 3′-UTR length for more than 800 genes in oocytes and most of them are favoring the longer 3′-UTR [14], however, the detailed biological outcomes and mechanisms are still elusive. Our findings that AREs-mediated HuR binding and stabilizing the longer 3′-UTR containing mRNA in YTHDC1 knockdown cells may provide a mechanism to explain how YTHDC1 regulates the RNA processes.

A reasonable hypothesis has been proposed that ferroptosis is a natural tumor suppressive mechanism contributing to the antitumor activity of the tumor suppressors [42]. In support of this hypothesis, several tumor suppressors, such as p53, BAP1 and fumarate hydratase (FH), exert their tumor suppressor's functions through ferroptosis [42–44]. Especially, the ferroptosis-promoting effect of p53 alone has been implied to be sufficient to suppress tumorigenesis in vivo [45]. Tumor cells do not undergo spontaneous ferroptosis unless the ferroptosis defense systems are damaged by GPX4 or FSP1 dysregulation [46]. Our results that the suppression of tumor cell growth by overexpression of YTHDC1 can be partially abrogated by ferroptosis inhibitor Fer-1 suggest that YTHDC1 regulates tumor progression at least partially through ferroptosis. We have further shown that YTHDC1-mediated FSP1 protein regulation may alter the FSP1-dependent ferroptosis surveillance system and, therefore, contributes to the tumor suppressor's activity of YTHDC1 in the lung cancer progression. However, whether there are other pathways (such as p53) and to what degree they are involved in YTHDC1's tumor-suppressive activity as well as which endogenous ferroptosis inducers that YTHDC1-FSP1 signaling axis responds warrant further investigation.

MATERIALS AND METHODS

Cell lines, animals, and reagents

The lung cancer cell lines A549, H1299, H1975, and H460 were obtained from the Cell Bank of the Chinese Academy of Science (Shanghai, China), and cultured in RPMI-1640 (Gibco, Life Technology, Carlsbad, CA, USA) supplemented with 10% fetal bovine serum (Gibco). All the cells were maintained at 37 °C with 5% CO_2. The male BALB/c-nude mice were purchased from the Vital River (Charles River China, Beijing, China). RSL3, Erastin, iFSP1, Fer-1 and Actinomycin D were purchased from MCE (New Jersey, USA). FIN56 and $FINO_2$ were purchased from Selleck (Texas, USA).

Tissue microarray (TMA) and immunohistochemical analysis

Tissue microarrays contained 98 lung cancer tissues (3 tissues were excluded from the analysis due to low tumor-cell content) were obtained from Shanghai Outdo Biotech Company (Shanghai, China) with the agreement of the patients with an informed consent form. IHC staining was performed using rabbit polyclonal antibody against YTHDC1 (Abcam, ab122340) or mouse monoclonal antibody against 4-HNE (Abcam, ab48506). Immunostaining was scored based on the extent of positive cell staining (0–100%) and the staining intensity (0, no staining; 1, slight staining; 2, moderate staining; and 3, strong staining). The final immunostaining score with a potential range of 0–300 was calculated as follows: Immunostaining score = [extent of positive cell staining (0–100%) × staining intensity (0–3)] × 100.

RNA extraction and qRT-PCR analysis

The total RNA was isolated using the Eastep Super Total RNA Extraction Kit (Promega, Shanghai, China), and the nuclear and cytoplasmic RNA of cells were isolated using PARIS™ Kit (Invitrogen, NY, USA) following the manufacturer's instructions. A total of 1000 ng RNA was used as a template for cDNA synthesis using PrimeScript™ RT reagent Kit with gDNA Eraser (TaKaRa, Dalian, China). Real-time PCR was performed using the SYBR Premix Ex Taq (TaKaRa). Results were normalized to the housekeeping gene *GAPDH* and relative gene expression levels were calculated using $2^{\wedge-(\Delta\Delta Ct)}$ method. Primers sequences were provided in Supplementary Table S4.

Plasmid construction and cell transfection

For YTHDC1 knockdown, shRNA and corresponding control lentiviruses were synthesized by GeneChem (Shanghai, China), and infected cells were selected using puromycin (2 μg/ml; Biosharp, Anhui, China). For YTHDC1 knockout, CRISPR/Cas9 and corresponding control lentiviruses were synthesized by GeneChem. For knockdown of FSP1, METTL3, and HuR, siRNAs targeting FSP1, METTL3 or HuR were purchased from the GenePharma (Shanghai, China). The siRNAs were transfected into cells with Lipofectamine 2000 (Invitrogen). To construct a plasmid expressing YTHDC1, the coding sequence of human YTHDC1 was synthesized and cloned into the GV492 vector (GeneChem). The lentivirus containing Flag-tagged YTHDC1 gene were transfected into cells and were screened under 2 μg/ml puromycin selection. YTHDC1 shRNA, YTHDC1 sgRNA, METTL3 siRNA, FSP1 siRNA, and HuR siRNA target sequences were shown in Supplementary Table S4.

Cell viability assay in vitro

The cell viability was detected using Cell Counting Kit-8 (CCK-8, Dojindo Laboratories, Kumamoto, Japan) assay, or CellTiter-Lumi™ Luminescent Cell Viability Assay Kit (Beyotime, Shanghai, China) based on quantification of adenosine triphosphate (ATP), which represented the number of active cells.

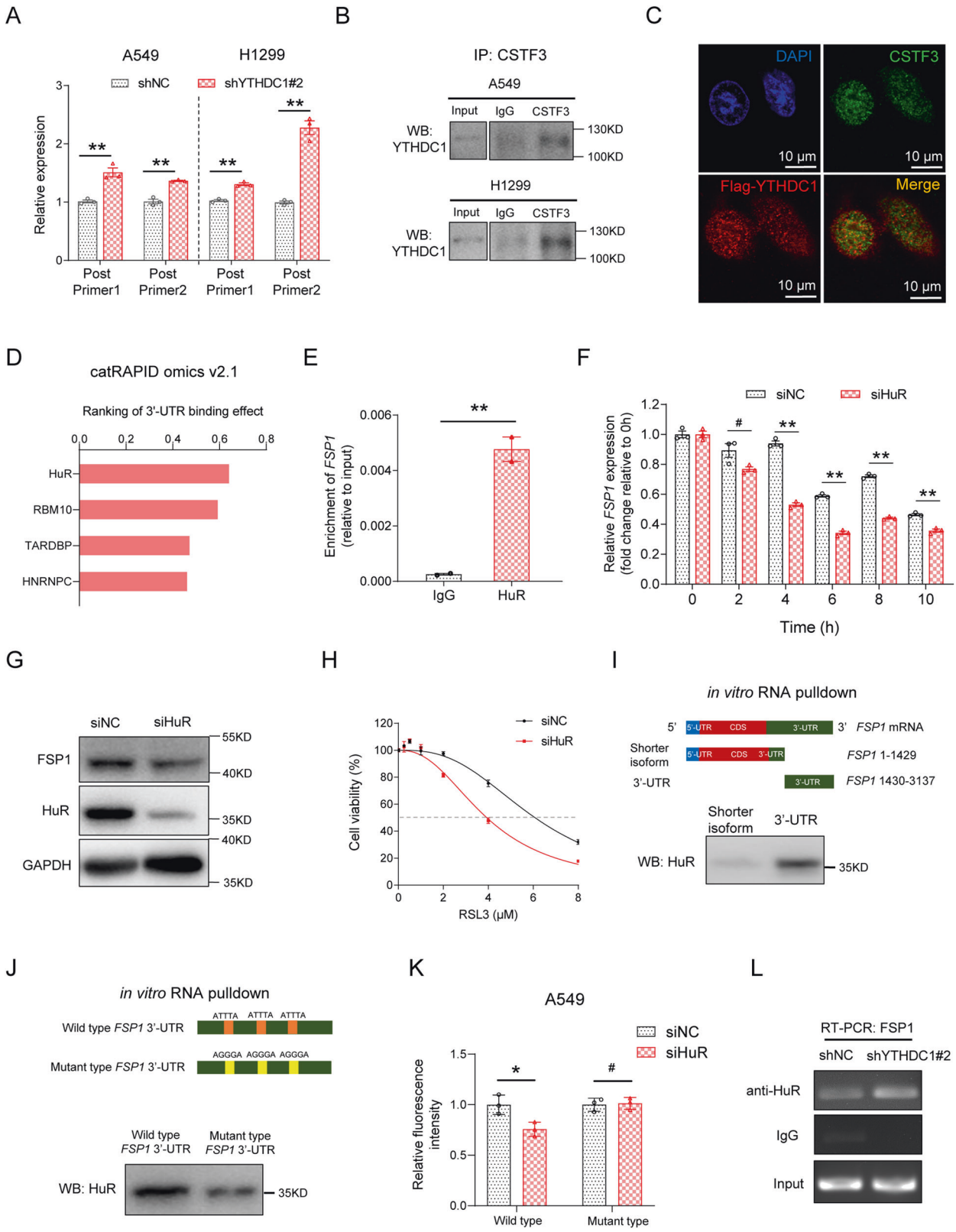

Colony formation assays

Cells were seeded in 6-well plates and media were changed every 3 days. Colonies were fixed with methanol and stained with 0.1% crystal violet (Beyotime) for 15 min. The visible colonies were then counted. All of the experiments were performed in triplicate.

Animal experiments in vivo

For subcutaneous xenograft model, ten 5 weeks old male BALB/c nude mice were randomly divided into two groups equally. Stable transfected A549 cells (5.0×10^6), suspended in 200 μL of 50% Matrigel (Corning, New York, USA), were injected subcutaneously into the flanks of the nude mice. The

Fig. 5 YTHDC1 knockdown regulates the alternative polyadenylation and increases the long isoform of *FSP1* mRNA, which can be bound and stabilized by HuR protein. A The longer isoform of *FSP1* mRNA is detected using two primers targeting 3′-UTR of *FSP1* mRNA in A549 and H1299 cells. The targeting sites of the primers are shown in Fig. 4D. **B** The binding effects of YTHDC1 and CSTF3 are detected by Co-IP assays in A549 and H1299 cells. **C** The co-localization of Flag-tagged YTHDC1 and CSTF3 are detected using a confocal microscopy in A549 cells. **D** The binding effect of *FSP1* mRNA 3′-UTR (*FSP1* mRNA region: 1430-3137) to the HuR, HNRNPC, TARDBP and RBM10 proteins are predicted using catRAPID omics v2.1. **E** The binding effect of *FSP1* mRNA by HuR protein is detected by RIP assay in A549 cells. **F** Stability of *FSP1* mRNA over 10 h is measured by qRT-PCR relative to time 0 h after blocking new RNA synthesis with Actinomycin D (5 μg/mL) in A549 cells after knockdown of HuR. **G** A549 cells are transfected with siRNAs targeting HuR, and FSP1 protein levels are detected using WB. **H** RSL3 treatment is conducted to clarify the effect of HuR on the ferroptosis in A549 cells. Cell proliferation is detected by CCK-8 assays and IC50 curves are generated using Graphpad Prism 8.0. **I** The binding region of *FSP1* mRNA by HuR protein is detected by RNA pulldown assays in A549 cells. **J** The binding effects of wild type and mutant 3′-UTR of *FSP1* mRNA to HuR protein are detected by RNA pulldown assays in A549 cells. **K** The binding effects of wild type and mutant 3′-UTR of *FSP1* mRNA to HuR protein are detected by Luciferase reporter assays in A549 cells. **L** The binding effects of *FSP1* mRNA by HuR protein are detected by RIP assays in A549 cells with stable knockdown of YTHDC1. Results are evaluated using the two-tailed Student's *t*-test. $^{\#}P > 0.05$; $^{*}P < 0.05$; $^{**}P < 0.01$.

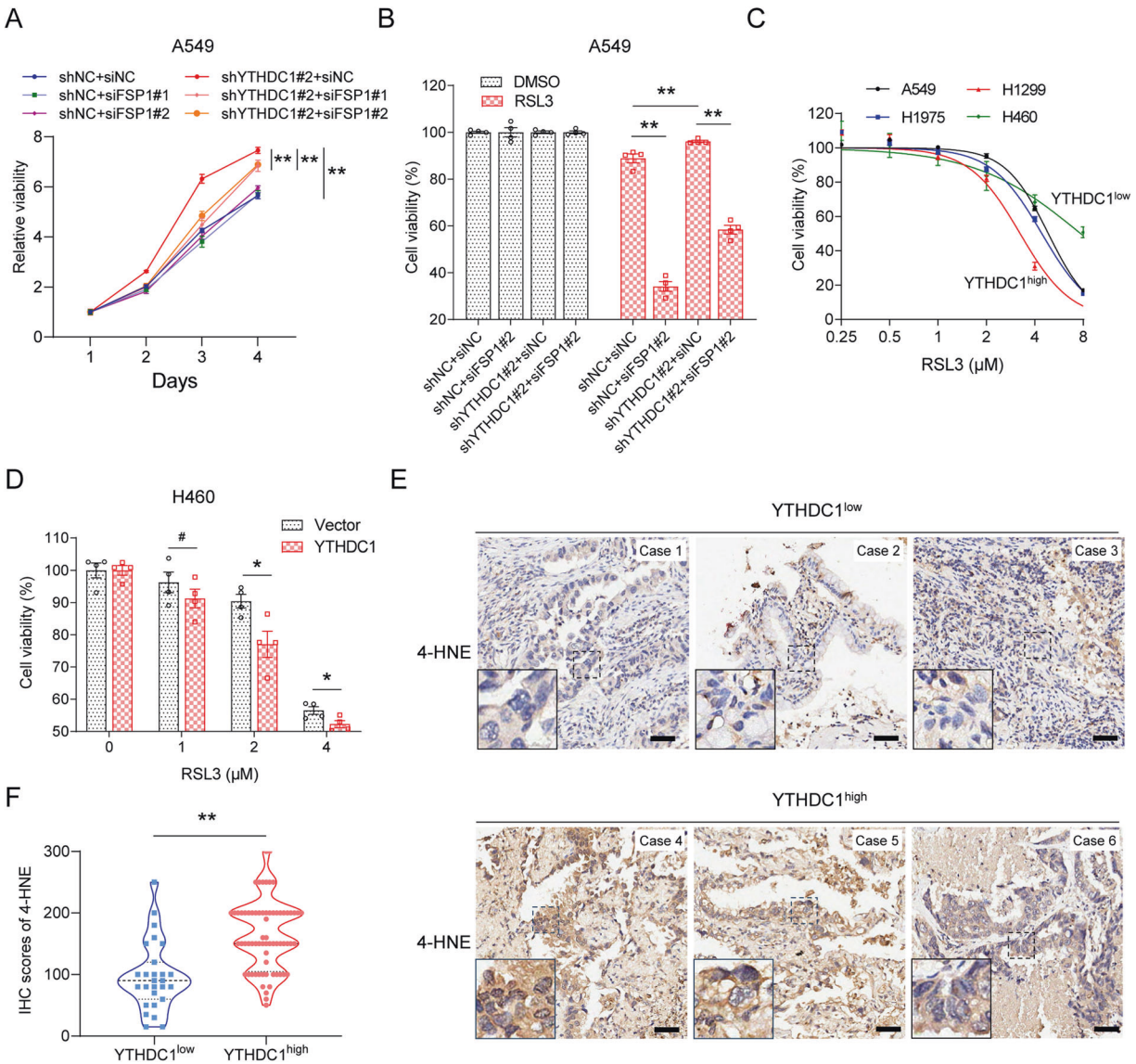

Fig. 6 YTHDC1 provides a ferroptotic vulnerability for lung cancer treatment. A Cell proliferation is detected by CCK-8 assays after transfection with siRNA targeting FSP1 in shNC and shYTHDC1 A549 cells. The difference between cell proliferation curves is evaluated using repeated measures analysis of variance. **B** RSL3 treatment is conducted to clarify the rescue effect of FSP1 on the ferroptosis resistance induced by YTHDC1 knockdown in A549 cells. Cell proliferation is detected by CCK-8 assays. Results are evaluated using the two-tailed Student's *t*-test. **C** RSL3 treatment is conducted to compare the ferroptosis sensitivity in lung cancer cells with different YTHDC1 protein levels. Cell proliferation is detected by CCK-8 assays and IC50 curves are generated using Graphpad Prism 8.0. **D** RSL3 treatment is conducted to compare the ferroptosis sensitivity in H460 cells after overexpression of YTHDC1. **E** Immunohistochemical staining of lung cancer tissues with 4-HNE in the same lung tumor tissues as Fig. 2A. Scale bars represent 50 μm. **F** IHC scores of 4-HNE in YTHDC1^{low} and YTHDC1^{high} lung tumor tissues are compared using Wilcoxon rank-sum test. YTHDC1^{low} and YTHDC1^{high} lung tumor tissues are defined as Fig. 2A. $^{\#}P > 0.05$; $^{*}P < 0.05$; $^{**}P < 0.01$.

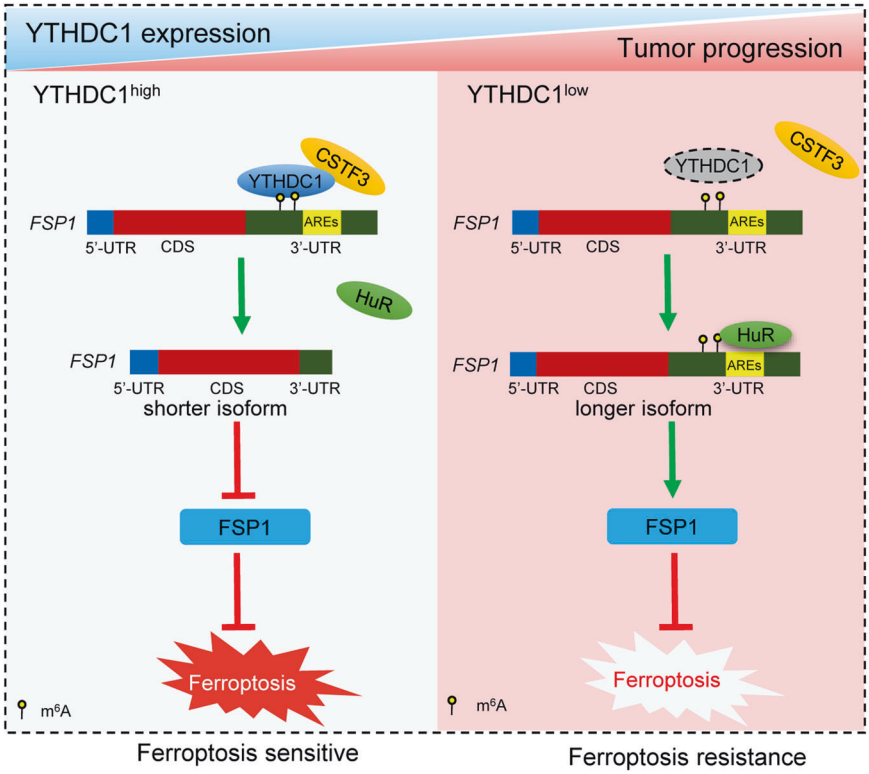

Fig. 7 A working model shows how YTHDC1 induces ferroptosis by regulating FSP1 in lung cancer. AREs AU-rich elements, UTR untranslated region.

tumor volumes were measured and were estimated by using the formula: $V = 0.5 \times D \times d^2$ (V, volume; D, longitudinal diameter; d, latitudinal diameter). The GFP fluorescent images of subcutaneous tumor were photographed and analyzed with Bruker Molecular Imaging Software (USA). All experimental animal procedures were approved by the Experimental Animal Welfare and Ethics, Zhongnan Hospital of Wuhan University.

Cellular ROS and lipid peroxidation measurement

For cellular ROS detection, cells (1×10^5) were grown in 6-well plates overnight and were then treated with RSL3 (800 nM) for 24 h, followed by the addition of DHE (KeyGEN BioTECH, Jiangsu, China) for 60 min. Cells were harvested and washed with PBS and then were subjected to flow cytometry to measure the levels of cellular ROS. For cellular lipid peroxidation detection, cells (1×10^5) were grown in 6-well plates overnight and were then treated with RSL3 (1 μM) for 24 h, followed by the addition of BODIPY 581/591 C11 (8 μM, ABclonal, Wuhan, China) for 60 min at 37 °C in the dark. Cells were harvested and washed with PBS and then were subjected to flow cytometry using the 488 nm and 561 nm laser for excitation. The BODIPY 581/591 C11 value was calculated as the ratio of the green fluorescence (which indicates oxidized probe) to total (green + red, which indicates total reduced plus oxidized probe) fluorescence.

RNA stability and Actinomycin D treatment

Cells (3.0×10^5) were seeded into 6-well plates overnight and were then treated with Actinomycin D (5 μg/mL), and then were harvested for RNA purification at 0, 2, 4, 6, 8, or 10 h. *FSP1* mRNA levels were subsequently measured by qRT-PCR to test whether YTHDC1 or HuR could regulate the stability of *FSP1* mRNA.

Transcriptome sequencing and analysis

The transcriptome sequencing was conducted at Shenzhen BGI. In brief, the total RNA was extracted from A549 cells and then the RNA was subjected to sequencing with DNBSEQ platform in the company of BGI (Shenzhen, China). The data were analyzed and visualized with the Dr. Tom System (BGI).

Luciferase reporter assay

To detect the HuR binding sites in the 3′-UTR of *FSP1* mRNA, the wild type (ATTTA) or mutant type (AGGGA) sequences of 3′-UTR of *FSP1* mRNA were inserted into the pmirGLO luciferase vectors. 5×10^3 A549 cells were seeded into 96-well plates in triplicate for each group. Cells were co-transfected with pmirGLO-*FSP1*-wild type 3′-UTR (or pmirGLO-*FSP1*- mutant type 3′-UTR) and siRNAs targeting HuR. Firefly and Renilla luciferase activities were measured at 48 h after transfection using the Dual-Luciferase Assay System (Beyotime) following the manufacturer's instructions. The relative luciferase activity was calculated using firefly/renilla luciferase activity.

Western blot and co-immunoprecipitation

Western blot (WB) and co-immunoprecipitation (Co-IP) were performed as described previously [47]. The antibodies used in this study were rabbit polyclonal antibody against YTHDC1 (1:1000; Abcam), rabbit monoclonal to GPX4 (1:1000; Abcam), rabbit monoclonal to HuR (1:1000; Abcam), rabbit monoclonal to GAPDH (1:1000; Abcam), mouse monoclonal to FSP1 (1:1000; Santa Cruz, USA), rabbit polyclonal to CSTF3 (1:1000; ABclonal), and mouse monoclonal to Caspase-3 (1:1000; Santa).

RNA immunoprecipitation assay and methylated RNA immunoprecipitation (MeRIP) assay

RNA immunoprecipitation (RIP) assay was performed using EZ-Magna RIP™ RNA-Binding Protein Immunoprecipitation Kit (Millipore, Billerica, MA, USA) following the manufacturer's protocol. In briefly, cells were lysed using the RIP lysis buffer. Immunoprecipitation were conducted with magnetic beads coupled with anti-HuR, anti-YTHDC1, or IgG. The enrichment of *FSP1* mRNA in immunoprecipitated RNAs was assessed by qRT-PCR assay. The methylated RNA immunoprecipitation (MeRIP) was performed to determine the m^6A levels in *FSP1* mRNA as described previously [48]. In briefly, 5 μg anti-m^6A antibody (ABclonal) or IgG were bound to magnetic beads (Magna RIP Kit, Millipore). A total of 50 μg RNA from the cells was immunoprecipitated with anti-m^6A antibody in RIP immunoprecipitation buffer (Magna RIP Kit, Millipore) overnight at 4 °C. After treating with proteinase K, RNA was extracted with an RNeasy Mini Kit (Qiagen). The enrichment of *FSP1* in m^6A immunoprecipitated RNAs was assessed by qRT-PCR assay.

RNA pull-down

Biotin-labeled *FSP1* mRNA was obtained through in vitro transcription from vector pcDNA3.1-*FSP1* mRNA 1-1429 and pcDNA3.1-*FSP1* mRNA 1430-3137

using Biotin RNA Labeling Mix (Roche, Mannheim, Germany) and T7 RNA polymerase (Roche). After treating with RNase-free DNase I (Promega), the biotin-labeled RNA was purified with an RNeasy Mini Kit (Qiagen, Germany) and then added into the A549 cell lysates. After incubating for 1 h, the biotin-labeled RNA was immunoprecipitated with Dynabeads™ M-270 Streptavidin (Invitrogen). Proteins were then eluted from the dynabeads and detected by WB.

Immunofluorescence cell staining and transmission electron microscopy

A549 cells transfected with Flag-tagged YTHDC1 fusion vector were grown on a sterile confocal petri dish (Biosharp), fixed in methanol for 15 min, permeabilized by 0.1% Triton X-100, and then blocked with 1% BSA for 30 min. Mouse anti-Flag (Sigma) and rabbit polyclonal to CSTF3 (ABclonal; A11665) were incubated overnight at 4 °C. After washing for three times, the cells were probed with Alexa-Fluor-555-conjugated goat anti-rabbit-IgG (Abcam) and Alexa-Fluor-647-conjugated goat anti-mouse-IgG (Abcam) for 1 h at room temperature, followed by nuclear counterstaining with DAPI (Beyotime). Cells were observed with a confocal fluorescence microscopy (Leica, Germany). For detecting the morphological changes of ferroptosis, cells were observed in a transmission electron microscopy (TEM) by Hitachi (HT7700 Exalens).

Bioinformatics analysis

To assess the clinical significance of YTHDC1 in lung cancer, the lung cancer RNA-seq data and clinical data were downloaded from the GTEx Portal (version V8) database and the Cancer Genome Atlas (TCGA) (version 2019-7-20). We compared the gene expression levels among patients subgrouped by tumor size, lymph node spread, and TNM stage. To evaluate the prognostic value of *YTHDC1*, Kaplan–Meier curves were generated using the Kaplan–Meier Plotter (KMplot) program (www.kmplot.com, version 2022). Four probes (228556_at, 212455_at, 214814_at and 240459_at) targeting YTHDC1 were used. The patients were classified into two groups using median gene expression value as the cutoff.

Statistical analysis

Statistical analyses were performed using the SPSS 19.0 software (SPSS, Inc., Chicago, IL, USA). Results were analyzed using the Wilcoxon rank-sum test, Student's *t*-test, Kruskal–Wallis test or repeated measures analysis of variance. A two-sided *P*-value less than 0.05 was taken as statistically significant.

DATA AVAILABILITY

All data needed to evaluate the conclusions are present in the paper and the supplementary files.

REFERENCES

1. Dixon SJ, Lemberg KM, Lamprecht MR, Skouta R, Zaitsev EM, Gleason CE, et al. Ferroptosis: an iron-dependent form of nonapoptotic cell death. Cell. 2012;149:1060–72.
2. Chen X, Li J, Kang R, Klionsky DJ, Tang D. Ferroptosis: machinery and regulation. Autophagy. 2021;17:2054–81.
3. Stockwell BR. A powerful cell-protection system prevents cell death by ferroptosis. Nature. 2019;575:597–8.
4. Li D, Li Y. The interaction between ferroptosis and lipid metabolism in cancer. Signal Transduct Target Ther. 2020;5:108.
5. Wu M, Xu LG, Su T, Tian Y, Zhai Z, Shu HB. AMID is a p53-inducible gene downregulated in tumors. Oncogene. 2004;23:6815–9.
6. Bersuker K, Hendricks JM, Li Z, Magtanong L, Ford B, Tang PH, et al. The CoQ oxidoreductase FSP1 acts parallel to GPX4 to inhibit ferroptosis. Nature. 2019;575:688–92.
7. Doll S, Freitas FP, Shah R, Aldrovandi M, da Silva MC, Ingold I, et al. FSP1 is a glutathione-independent ferroptosis suppressor. Nature. 2019;575:693–8.
8. He PC, He C. m(6) A RNA methylation: from mechanisms to therapeutic potential. EMBO J. 2021;40:e105977.
9. Lan Q, Liu PY, Bell JL, Wang JY, Huttelmaier S, Zhang XD, et al. The emerging roles of RNA m(6)A methylation and demethylation as critical regulators of tumorigenesis, drug sensitivity, and resistance. Cancer Res. 2021;81:3431–40.
10. Shi H, Wei J, He C. Where, when, and how: context-dependent functions of RNA methylation writers, readers, and erasers. Mol Cell. 2019;74:640–50.
11. Widagdo J, Anggono V, Wong JJ. The multifaceted effects of YTHDC1-mediated nuclear m(6)A recognition. Trends Genet. 2022;38:325–32.
12. Chen C, Liu W, Guo J, Liu Y, Liu X, Liu J, et al. Nuclear m(6)A reader YTHDC1 regulates the scaffold function of LINE1 RNA in mouse ESCs and early embryos. Protein Cell. 2021;12:455–74.
13. Liu J, Gao M, He J, Wu K, Lin S, Jin L, et al. The RNA m(6)A reader YTHDC1 silences retrotransposons and guards ES cell identity. Nature. 2021;591:322–6.
14. Kasowitz SD, Ma J, Anderson SJ, Leu NA, Xu Y, Gregory BD, et al. Nuclear m6A reader YTHDC1 regulates alternative polyadenylation and splicing during mouse oocyte development. PLoS Genet. 2018;14:e1007412.
15. Sheng Y, Wei J, Yu F, Xu H, Yu C, Wu Q, et al. A critical role of nuclear m6A reader YTHDC1 in leukemogenesis by regulating MCM complex-mediated DNA replication. Blood. 2021;138:2838–52.
16. Ma J, Yang D, Ma XX. Immune infiltration-related N6-methyladenosine RNA methylation regulators influence the malignancy and prognosis of endometrial cancer. Aging (Albany NY). 2021;13:16287–315.
17. Cheng Y, Xie W, Pickering BF, Chu KL, Savino AM, Yang X, et al. N(6)-Methyladenosine on mRNA facilitates a phase-separated nuclear body that suppresses myeloid leukemic differentiation. Cancer Cell. 2021;39:958–972.e958.
18. Li S, Qi Y, Yu J, Hao Y, He B, Zhang M, et al. Nuclear Aurora kinase A switches m(6)A reader YTHDC1 to enhance an oncogenic RNA splicing of tumor suppressor RBM4. Signal Transduct Target Ther. 2022;7:97.
19. Yan H, Zhang L, Cui X, Zheng S, Li R. Roles and mechanisms of the m(6)A reader YTHDC1 in biological processes and diseases. Cell Death Discov. 2022;8:237.
20. Huang H, Weng H, Chen J. m(6)A modification in coding and non-coding RNAs: roles and therapeutic implications in cancer. Cancer Cell. 2020;37:270–88.
21. Yang WS, SriRamaratnam R, Welsch ME, Shimada K, Skouta R, Viswanathan VS, et al. Regulation of ferroptotic cancer cell death by GPX4. Cell. 2014;156:317–31.
22. Xie Y, Hou W, Song X, Yu Y, Huang J, Sun X, et al. Ferroptosis: process and function. Cell Death Differ. 2016;23:369–79.
23. Jiang X, Stockwell BR, Conrad M. Ferroptosis: mechanisms, biology and role in disease. Nat Rev Mol Cell Biol. 2021;22:266–82.
24. Kim GW, Imam H, Siddiqui A. The RNA binding proteins YTHDC1 and FMRP regulate the nuclear export of N(6)-methyladenosine-modified hepatitis B virus transcripts and affect the viral life cycle. J Virol. 2021;95:e0009721.
25. Roundtree IA, Luo GZ, Zhang Z, Wang X, Zhou T, Cui Y, et al. YTHDC1 mediates nuclear export of N(6)-methyladenosine methylated mRNAs. Elife. 2017;6:e31311.
26. Li F, Yi Y, Miao Y, Long W, Long T, Chen S, et al. N(6)-methyladenosine modulates nonsense-mediated mRNA decay in human glioblastoma. Cancer Res. 2019;79:5785–98.
27. Zhang Y, Liu L, Qiu Q, Zhou Q, Ding J, Lu Y, et al. Alternative polyadenylation: methods, mechanism, function, and role in cancer. J Exp Clin Cancer Res. 2021;40:51.
28. Liu H, Moore CL. On the cutting edge: regulation and therapeutic potential of the mRNA 3′ end nuclease. Trends Biochem Sci. 2021;46:772–84.
29. Mohanan NK, Shaji F, Koshre GR, Laishram RS. Alternative polyadenylation: an enigma of transcript length variation in health and disease. Wiley Interdiscip Rev RNA. 2022;13:e1692.
30. Wu X, Xu L. The RNA-binding protein HuR in human cancer: a friend or foe? Adv Drug Deliv Rev. 2022;184:114179.
31. Lee JH, Wang R, Xiong F, Krakowiak J, Liao Z, Nguyen PT, et al. Enhancer RNA m6A methylation facilitates transcriptional condensate formation and gene activation. Mol Cell. 2021;81:3368–3385.e3369.
32. Su Y, Wang B, Huang J, Huang M, Lin T. YTHDC1 positively regulates PTEN expression and plays a critical role in cisplatin resistance of bladder cancer. Cell Prolif. 2023;56:e13404.
33. Stockwell BR, Friedmann Angeli JP, Bayir H, Bush AI, Conrad M, Dixon SJ, et al. Ferroptosis: a regulated cell death nexus linking metabolism, redox biology, and disease. Cell. 2017;171:273–85.
34. Chen X, Kang R, Kroemer G, Tang D. Organelle-specific regulation of ferroptosis. Cell Death Differ. 2021;28:2843–56.
35. Li W, Liang L, Liu S, Yi H, Zhou Y. FSP1: a key regulator of ferroptosis. Trends Mol Med. 2023;29:753-64.
36. Dos Santos AF, Fazeli G, Xavier da Silva TN, Friedmann Angeli JP. Ferroptosis: mechanisms and implications for cancer development and therapy response. Trends Cell Biol. 2023; https://doi.org/10.1016/j.tcb.2023.04.005. Epub ahead of print.
37. Koppula P, Lei G, Zhang Y, Yan Y, Mao C, Kondiparthi L, et al. A targetable CoQ-FSP1 axis drives ferroptosis- and radiation-resistance in KEAP1 inactive lung cancers. Nat Commun. 2022;13:2206.
38. Sommerkamp P, Cabezas-Wallscheid N, Trumpp A. Alternative polyadenylation in stem cell self-renewal and differentiation. Trends Mol Med. 2021;27:660–72.
39. Davis AG, Johnson DT, Zheng D, Wang R, Jayne ND, Liu M, et al. Alternative polyadenylation dysregulation contributes to the differentiation block of acute myeloid leukemia. Blood. 2022;139:424–38.

40. Tang P, Yang Y, Li G, Huang L, Wen M, Ruan W, et al. Alternative polyadenylation by sequential activation of distal and proximal PolyA sites. Nat Struct Mol Biol. 2022;29:21–31.
41. Ma W, Mayr C. A membraneless organelle associated with the endoplasmic reticulum enables 3'UTR-mediated protein-protein interactions. Cell. 2018;175:1492–1506.e1419.
42. Gao M, Yi J, Zhu J, Minikes AM, Monian P, Thompson CB, et al. Role of mitochondria in ferroptosis. Mol Cell. 2019;73:354–363.e353.
43. Jiang L, Kon N, Li T, Wang SJ, Su T, Hibshoosh H, et al. Ferroptosis as a p53-mediated activity during tumour suppression. Nature. 2015;520:57–62.
44. Zhang Y, Shi J, Liu X, Feng L, Gong Z, Koppula P, et al. BAP1 links metabolic regulation of ferroptosis to tumour suppression. Nat Cell Biol. 2018;20:1181–92.
45. Wang SJ, Li D, Ou Y, Jiang L, Chen Y, Zhao Y, et al. Acetylation is crucial for p53-mediated ferroptosis and tumor suppression. Cell Rep. 2016;17:366–73.
46. Liang D, Feng Y, Zandkarimi F, Wang H, Zhang Z, Kim J, et al. Ferroptosis surveillance independent of GPX4 and differentially regulated by sex hormones. Cell. 2023;186:2748–2764.e2722.
47. Yuan S, Yu Z, Liu Q, Zhang M, Xiang Y, Wu N, et al. GPC5, a novel epigenetically silenced tumor suppressor, inhibits tumor growth by suppressing Wnt/beta-catenin signaling in lung adenocarcinoma. Oncogene. 2016;35:6120–31.
48. Song T, Yang Y, Wei H, Xie X, Lu J, Zeng Q, et al. Zfp217 mediates m6A mRNA methylation to orchestrate transcriptional and post-transcriptional regulation to promote adipogenic differentiation. Nucleic Acids Res. 2019;47:6130–44.

AUTHOR CONTRIBUTIONS

HH led the study by designing, interpreting results, obtaining the funding and reviewing the manuscript. SY, SX, and HW participated in performing the experiments, results interpretation, manuscript writing. MMG, JHZ, ZPY, HZ, ZY, ZX, DJM, RKS, YZ, and TZ participated in performing the experiments and collecting the data. MYL performed the bioinformatics analysis and participated in results interpretation. GL and XH participated in the manuscript discussion. YL and XTZ participated in study design, results interpretation and reviewing the manuscript.

FUNDING

This work was supported by the National Natural Science Foundation of China (No. 82002447 to SY; 82173131 to HH), the Outstanding Young and Middle-aged Talents Training Program of Zhongnan Hospital of Wuhan University (Grant No. ZNYQ2022003 to SY), the Science and Technology Innovation Commission of Shenzhen Municipal Government Grants (JCYJ20210324104007022 to HH), Guangdong provincial fundings: 2021KTSCX108 (to XH), and the Program of Excellent Doctoral (Postdoctoral) of Zhongnan Hospital of Wuhan University (No. ZNYB2020028 to SY).

COMPETING INTERESTS

The authors declare no competing interests.

ETHICS

All experimental animal procedures were approved by the Experimental Animal Welfare and Ethics, Zhongnan Hospital of Wuhan University.

ADDITIONAL INFORMATION

Supplementary information The online version contains supplementary material available at https://doi.org/10.1038/s41418-023-01234-w.

Correspondence and requests for materials should be addressed to Yafei Li, Xian-Tao Zeng or Hailiang Hu.